

Inflationary Potential from 21 cm Tomography and Planck

Vernon Barger¹, Yu Gao¹, Yi Mao^{2,3} and Danny Marfatia⁴

¹*Department of Physics, University of Wisconsin, Madison, WI 53706*

²*Department of Physics, Massachusetts Institute of Technology, Cambridge, MA 02139*

³*Department of Astronomy, University of Texas, Austin, TX 78712*

⁴*Department of Physics and Astronomy, University of Kansas, Lawrence, KS 66045*

Abstract

Three-dimensional neutral hydrogen mapping using the redshifted 21 cm line has recently emerged as a promising cosmological probe. Within the framework of slow-roll reconstruction, we analyze how well the inflationary potential can be reconstructed by combining data from 21 cm experiments and cosmic microwave background data from the Planck satellite. We consider inflationary models classified according to the amplitude of their tensor component, and show that 21 cm measurements can significantly improve constraints on the slow-roll parameters and determine the shape of the inflationary potential.

1 Introduction

Inflation is the prominent paradigm of the early universe that explains the flatness over cosmological scales, the Gaussianity of density perturbations and the near scale invariance of the cosmic power spectrum. Accelerated cosmic expansion during inflation pushes perturbation modes from casually connected scales to outside the horizon. After re-entering the horizon these superhorizon modes provide homogeneity over apparently casually disconnected scales, and give rise to the peaks in the power spectrum of the cosmic microwave background (CMB) radiation which has been measured with unprecedented precision over a five-year period by the Wilkinson Microwave Anisotropy Probe (WMAP5) [1]. The Planck [2] satellite, planned to be launched in 2009, and continued observation by WMAP will further exploit the rich information from both CMB temperature and polarization power spectra.

However, the mechanism that drives the early universe into inflation remains an open question. Generically inflation can be modelled by an inflationary field rolling down a potential [3, 4]. Models may be large field [5], small field [6] and hybrid [7] and have been widely studied. Alternatively an inverse method [8] focuses solely on the kinematics of rolling and reconstructs the inflationary potential in a model-independent manner. The slow-roll parameters are defined in terms of the derivatives of the potential. These parameters can determine the primordial power spectrum that sheds light on how well the inflationary potential can be experimentally probed. Slow-roll parameters have been utilized lately to analyze inflation with WMAP data [9] and the upcoming Planck project [10, 11].

A number of radio telescopes are currently being proposed, planned or constructed to observe the redshifted 21 cm hydrogen line from the Epoch of Reionization (EoR), *e.g.*, MWA [12], 21CMA [13], LOFAR [14], GMRT [15], PAPER [16], Square Kilometer Array (SKA) [17], and Fast Fourier Transform Telescope (FFTT) [18]. 21 cm tomography maps the neutral hydrogen in the universe over a wide range of redshifts and provides a promising cosmological probe, with arguably greater potential than CMB and galaxy surveys. Several studies have investigated the accuracies with which cosmological parameters can be measured by upcoming 21 cm experiments, both by mapping diffuse hydrogen before and during the EoR [19] and by mapping neutral hydrogen in the galactic halo after reionization [20]. In particular, the FFTT experiment optimized for 21 cm tomography can improve measurement of the cosmological parameters to an unprecedented level [21]. Consequently, precision measurements from 21 cm tomography open a new window to constrain inflation in the early universe.

In this paper, we adopt a model-independent approach and forecast how accurately the shape of the inflationary potential can be reconstructed by combining the 21 cm data from FFTT or SKA and the CMB data from Planck. In the next two sections we outline the reconstruction method

and assumptions about the 21 cm power spectrum. In Sections 4 and 5, we describe the two classes of kinematical models and their analysis. We display our results in Section 6.

2 Potential reconstruction

We briefly outline the potential reconstruction method and refer the reader to Refs. [23, 24] for extensive discussions.

Consider a flat universe whose energy-momentum tensor is dominated by an inflaton field ϕ evolving monotonically with time in a potential $V(\phi)$. With the Hubble parameter H expressed in terms of ϕ , the equation of motion of ϕ and the Friedmann equation can be written as

$$\dot{\phi} = -\frac{m_{\text{Pl}}^2}{4\pi} H'(\phi), \quad (1)$$

and

$$V(\phi) = \frac{3m_{\text{Pl}}^2}{8\pi} H^2(\phi) \left[1 - \frac{1}{3}\epsilon(\phi) \right], \quad (2)$$

where m_{Pl} is the Planck mass, primes and overdots denote derivatives with respect to ϕ and time, respectively, and

$$\epsilon(\phi) = \frac{m_{\text{Pl}}^2}{4\pi} \left(\frac{H'(\phi)}{H(\phi)} \right)^2. \quad (3)$$

Inflation occurs so long as $\epsilon < 1$.

A series of higher order parameters are obtained by successive differentiation [25]:

$$\lambda_n = \left(\frac{m_{\text{Pl}}^2}{4\pi} \right)^n \frac{(H'(\phi))^{n-1} H^{(n+1)}(\phi)}{H^n(\phi)}, \quad (4)$$

where $n \geq 1$ and the usual slow-roll parameters are $\eta = \lambda_1$ and $\xi = \lambda_2$. No assumption of slow-roll is made in the definition of these parameters. If the hierarchy of differential equations is truncated so that $\lambda_n = 0$ for $n \geq m$, an exact solution for $H(\phi)$ (up to a normalization factor) can be found [26]. Once $H(\phi)$ is known, the shape of the potential $V(\phi)$ is determined.

The evolution of the slow-roll parameters is conveniently expressed as a function of the number of e-folds before the end of inflation N . With

$$\left(\frac{dN}{d\phi} \right)^2 = \frac{4\pi}{m_{\text{Pl}}^2 \epsilon(\phi)}, \quad (5)$$

the flow of the slow-roll parameters is given by [4]

$$\frac{d\epsilon}{dN} = 2\epsilon(\lambda_1 - \epsilon), \quad (6)$$

$$\frac{d\lambda_n}{dN} = [(n-1)\lambda_1 - n\epsilon] \lambda_n + \lambda_{n+1}. \quad (7)$$

To solve these equations, we need to specify values of the slow-roll parameters when observable modes left the horizon. We denote these by a “0” subscript and take $k_0 = 0.05 \text{ Mpc}^{-1}$ to be the fiducial mode. We set $\phi_0 = 0$.

The spectral indices and their running that define the commonly used power-law parameterization of the primordial scalar and tensor power spectra [27]

$$P_s(k) = A_s \left(\frac{k}{k_0} \right)^{n_s - 1 + \frac{1}{2} \alpha \ln \frac{k}{k_0}}, \quad (8)$$

$$P_t(k) = A_t \left(\frac{k}{k_0} \right)^{n_t}, \quad (9)$$

can be related to the slow-roll parameters. To second order, expressions for parameters that will be relevant to our study, are [24]

$$n_s = 1 + 2\eta_0 - 4\epsilon_0 - 2(1 + C)\epsilon_0^2 - \frac{1}{2}(3 - 5C)\epsilon_0\eta_0 + \frac{1}{2}(3 - C)\xi_0, \quad (10)$$

$$\alpha = \left. \frac{dn_s}{d \ln k} \right|_0 = - \left. \frac{1}{1 - \epsilon_0} \frac{dn_s}{dN} \right|_0, \quad (11)$$

where $C = 4(\ln 2 + \gamma) - 5$, with $\gamma \sim 0.577$, and the tensor to scalar ratio $r = A_t/A_s$ is

$$r = 16\epsilon_0[1 + 2(-2 + \ln 2 + \gamma)(\epsilon_0 - \eta_0)]. \quad (12)$$

WMAP5 data support a red-tilted ($n_s < 1$) spectrum and $r < 0.25$ [1]. With A_s fixed by observation, the parameter r determines the tensor amplitude. If $r \gtrsim 0.1$, tensor modes are detectable by Planck [28].

3 21 cm power spectrum

We briefly describe the essential background of 21cm cosmology in this section, and refer the interested reader to a comprehensive review in Ref. [29]. The redshifted 21 cm line due to the neutral hydrogen hyperfine transition can be measured in terms of the brightness temperature relative to the CMB temperature [30],

$$T_b(\mathbf{x}) = \frac{3c^3 h A_{10} n_H(\mathbf{x}) [T_S(\mathbf{x}) - T_{CMB}]}{32\pi k_B \nu_0^2 T_S(\mathbf{x}) (1+z)^2 \partial v_{\parallel} / \partial r}, \quad (13)$$

where A_{10} is the spontaneous decay rate of 21 cm transition, n_H is the number density of the neutral hydrogen gas, T_S is the spin temperature and $\partial v_{\parallel} / \partial r$ is the physical velocity gradient along the line of sight (with r the comoving distance). The temperature fluctuation can be parametrized in terms of the fluctuation in the ionized fraction δ_x , the matter density fluctuation δ , and the gradient of peculiar velocity along the line of sight dv_r/dr . During the EoR, the hydrogen gas is

heated well above the CMB temperature [31], so that in the approximation $T_s \gg T_{\text{CMB}}$,

$$T_b = \frac{\langle T_b \rangle}{\langle x_H \rangle} [1 - \langle x_i \rangle (1 + \delta_x)] (1 + \delta) \left(1 - \frac{1}{Ha} \frac{dv_r}{dr} \right), \quad (14)$$

where $x_i = 1 - x_H$ is the ionized fraction of hydrogen gas and x_H is the fraction of neutral hydrogen. The total 21 cm power spectrum $P_{\Delta T}(\mathbf{k})$ is defined by $\langle \Delta T_b^*(\mathbf{k}) \Delta T_b(\mathbf{k}') \rangle \equiv (2\pi)^3 \delta^3(\mathbf{k} - \mathbf{k}') P_{\Delta T}(\mathbf{k})$, where $\Delta T_b(\mathbf{k})$ is the deviation from the mean brightness temperature and \mathbf{k} is the comoving wave-vector that is the Fourier dual of the real coordinate position \mathbf{r} . We restrict our considerations to linear perturbation theory ($\delta \ll 1$) and write the Fourier transformed spectrum to leading order as

$$P_{\Delta T}(\mathbf{k}) = P_0(k) + P_2(k)\mu^2 + P_4(k)\mu^4, \quad (15)$$

where the multipole coefficients can be written as

$$P_0 = \mathcal{P}_{\delta\delta} - 2\mathcal{P}_{x\delta} + \mathcal{P}_{xx}, \quad (16)$$

$$P_2 = 2(\mathcal{P}_{\delta\delta} - \mathcal{P}_{x\delta}), \quad (17)$$

$$P_4 = \mathcal{P}_{\delta\delta}. \quad (18)$$

Here $\mu = \hat{\mathbf{k}} \cdot \hat{\mathbf{n}}$ is the cosine of angle between the wave-vector and the line of sight. The power spectra of matter and ionization fluctuations are denoted by $\mathcal{P}_{\delta\delta} = \tilde{T}_b^2 \langle x_H \rangle^2 P_{\delta\delta}$, $\mathcal{P}_{x\delta} = \tilde{T}_b^2 \langle x_H \rangle \langle x_i \rangle P_{\delta x}$, and $\mathcal{P}_{xx} = \tilde{T}_b^2 \langle x_i \rangle^2 P_{\delta x \delta x}$, where $\tilde{T}_b \equiv \frac{\langle T_s \rangle}{\langle T_s \rangle - T_{\text{CMB}}} \frac{\langle T_b \rangle}{\langle x_H \rangle} \approx \frac{\langle T_b \rangle}{\langle x_H \rangle}$. We account for ionization effects by parameterizing the ionization power spectra as [21]

$$\mathcal{P}_{xx}(k) = b_{xx}^2 [1 + \alpha_{xx}(k R_{xx}) + (k R_{xx})^2]^{-\frac{\gamma_{xx}}{2}} \mathcal{P}_{\delta\delta}, \quad (19)$$

$$\mathcal{P}_{x\delta}(k) = b_{x\delta}^2 \exp[-\alpha_{x\delta}(k R_{x\delta}) - (k R_{x\delta})^2] \mathcal{P}_{\delta\delta}, \quad (20)$$

where b_{xx}^2 and $b_{x\delta}^2$ are the amplitudes of the spectra, R_{xx} and $R_{x\delta}$ are the effective sizes of the ionized bubbles (HII regions), and α_{xx} , γ_{xx} and $\alpha_{x\delta}$ are spectral indices. We adopt the fiducial values of Table III in Ref. [21].

4 Model classification

Kinematically different potentials can be categorized based on the relative sizes of slow-roll parameters. The parameter ϵ plays a critical role that determines the duration of inflation, the rate of change of ϕ , how much the inflationary potential $V(\phi)$ rolls down from its initial height, and the tensor to scalar ratio. We follow a recent classification that is based on the size of ϵ [11].

4.1 High ϵ models.

High ϵ models yield $r \gtrsim 0.1$ so that tensor modes are detectable by Planck.

One-parameter models. ϵ is the sole parameter in these models and determines the primordial spectra. As the only free parameter, ϵ is stringently constrained by 21 cm and CMB data. However, this single parameter scenario is not easily realized in particle physics.

Two-parameter models. In these models η contributes to the evolution equations. Two-parameter models resemble a Λ CDM cosmology with significant tensor power.

Three-parameter models. Inflationary rolling is described by ϵ , η and ξ . These models resemble a Λ CDM model with measurable r and a large ξ can contribute significantly to the running of scalar spectral index α , breaking scale invariance of the power spectrum. The non-zero ξ allows the rolling to speed up at late times and gives a variety of shapes for the potential. ξ contributes significantly to α when it is numerically comparable to the other two parameters. Generically, ξ speeds up the evolution of ϵ and a large ξ causes a prompt end to inflation with small N .

4.2 Low ϵ models.

In these models ϵ is vanishingly small when k_0 leaves the horizon. We set $\epsilon_0 = 10^{-8}$. This represents extremely slow rolling at horizon-crossing. In such models non-zero higher order parameters cause ϵ to grow super-exponentially near the end of inflation and the potential falls abruptly with a cliff-like feature.

Two-parameter models. These models resemble Λ CDM with near scale invariance in the power spectrum and negligible tensors. The parameter η can be strongly constrained but the number of e-folds are generally large because an efficient accelerating mechanism is absent. Within 95% C. L. constraints from WMAP5, we find that these models give $N > 180$. A large N indicates that inflation must end via a hybrid transition.

Three-parameter models. A non-zero ξ parameter speeds up rolling, significantly lowers the number of e-folds and allows a non-zero α . These models can easily be distinguished from the two-parameter case. It is noteworthy that in these models it is possible for rolling to be even slower than in two-parameter models during most of the inflationary period. This is followed by significant late-time acceleration which causes the overall effect of ξ to be a speed-up of rolling. The phase of slow evolution also occurs in models with higher order kinematical parameters.

Here we do not investigate low ϵ models with higher order parameters (λ_n with $n \geq 3$) since such models are indistinguishable from the three-parameter model.

5 Analysis

21 cm experiments do not directly measure \mathbf{k} or $P_{\Delta T}(\mathbf{k})$. The power spectrum $P_{\Delta T}(\mathbf{u})$ is evaluated in the observer’s pixel \mathbf{u} that is the Fourier dual of the observed vector $\Theta \equiv \theta_x \hat{x} + \theta_y \hat{y} + \Delta\nu \hat{z}$ where (θ_x, θ_y) gives the angular location on the sky plane, $\Delta\nu$ is the frequency difference from the central redshift of a data bin and the z -axis is along the line of sight. By using $P_{\Delta T}(\mathbf{u})$ instead of $P_{\Delta T}(\mathbf{k})$, we avoid the Alcock-Paczynski effect [32], which arises from the model dependence in the projection of the physical wave-vector \mathbf{k} over cosmological distances.

We employ the Fisher matrix formalism to determine the precision of parameter estimation. Following Ref. [21], we resolve the 21 cm spectrum $P_{\Delta T}(\mathbf{u})$ into pixels and the 21 cm Fisher matrix is constructed as

$$\mathbf{F}_{ab}^{21cm} = \sum_{pixels} \frac{1}{[\delta P_{\Delta T}(\mathbf{u})]^2} \left(\frac{\partial P_{\Delta T}(\mathbf{u})}{\partial \lambda_a} \right) \left(\frac{\partial P_{\Delta T}(\mathbf{u})}{\partial \lambda_b} \right), \quad (21)$$

where $\delta P_{\Delta T}(\mathbf{u})$ is the power spectrum measurement error in a pixel at \mathbf{u} and λ is the combined set of cosmological and ionization parameters.

We consider 21 cm measurements in the redshift range 6.8–8.2 with three redshift bins centered at $z = 7.0, 7.5$ and 8.0 , with a nonlinear cut-off scale $k_{max} = 2 \text{ Mpc}^{-1}$, and 16000 observation hours. Non-Gaussianity of ionization signals is assumed to be negligible in our analysis. We assume that the foreground can be perfectly cleaned above the scale $k_{min} = 2\pi/yB$ where yB is the comoving line-of-sight distance width of a single redshift bin. This assumption was shown to be a good approximation in Ref. [19]. We consider two detector arrays, SKA and FFTT, which have optimal signal-to-noise ratios among planned 21 cm experiments. We assume an azimuthally symmetric distribution of baselines in both arrays. The design of SKA has not been finalized. We adopt the “smaller antennae” version of SKA, in which the array will have 7000 10 m antennae. We assume that 16% of the antennae are concentrated in a nucleus within which the area coverage fraction is close to 100%; 4% of the antennae have a coverage density that falls as the inverse square of the radius; and 30% are in the annulus where the coverage density is low but rather uniform out to a 5 km radius. We ignore the measurements from the sparse distribution of the remaining 50% of the antenna panels that are outside the annulus. FFTT is a future square kilometer array optimized for 21 cm tomography as described in Ref. [18]. Unlike other interferometers, which add in phase the dipoles in each panel or station, FFTT can obtain more information by correlating all of its dipoles. We assume that FFTT contains a million $1 \text{ m} \times 1 \text{ m}$ dipole antennae in a contiguous core subtending a square kilometer, and providing a field-of-view of 2π steradians.

The Fisher matrix formalism for the CMB is well established [33]; for Planck data we follow the latest experimental specifications [2]. We include both temperature and polarization measurements and assume $l_{max} = 3000$ with three frequency channels while the other channels are used for

foreground subtraction. The CMB power spectra’s parameter dependence is computed using the Code for Anisotropies in the Microwave Background (CAMB) [34].

The Fisher matrix is cosmology dependent and we work in the flat ($\Omega_k = 0$) standard Λ CDM model and fix $\Omega_\nu h^2 = 0.0074$ (neutrino density) and $Y_p = 0.24$ (helium abundance). The fiducial values of the non-slow-roll parameters are set near the best-fit of the WMAP5 result [1]: $h = 0.72$ (Hubble parameter $H_0 \equiv 100h \text{ km s}^{-1} \text{ Mpc}^{-1}$), $\tau = 0.087$ (reionization optical depth), $\Omega_\Lambda = 0.742$ (dark energy density), $\Omega_b h^2 = 0.02273$ (physical baryon density), and $A_s = 0.9$. We fix $\mathcal{P}_{\delta\delta}(k)$ in Eqs. (19) and (20) when varying cosmological parameters, so that constraints arise only from the $\mathcal{P}_{\delta\delta}$ terms in P_0 , P_2 and P_4 .

The Fisher matrices depend on $\boldsymbol{\lambda}$ that includes (n_s, r, α) in \mathbf{F}^{Planck} and (n_s, α) in \mathbf{F}^{21cm} in addition to the non-inflationary parameters. We marginalize over the latter to obtain $\mathbf{F}_{(n_s, r, \alpha)}^{Planck}$ and $\mathbf{F}_{(n_s, \alpha)}^{21cm}$. The Jacobian matrix $\partial\boldsymbol{\lambda}_{spec}/\partial\boldsymbol{\lambda}_{sr}$ (where the subscript “spec” indicates (n_s, r, α) for Planck and (n_s, α) for 21 cm experiments), can be used to obtain the Fisher matrices for the slow-roll parameter set $\boldsymbol{\lambda}_{sr} \equiv (\epsilon, \eta, \xi)$,

$$\mathbf{F}_{sr} = \left(\frac{\partial\boldsymbol{\lambda}_{spec}}{\partial\boldsymbol{\lambda}_{sr}} \right)^T \mathbf{F}_{spec} \frac{\partial\boldsymbol{\lambda}_{spec}}{\partial\boldsymbol{\lambda}_{sr}}. \quad (22)$$

The three independent spectral parameters allow the Jacobian matrix a maximal rank of three, and directly constrain up to three slow-roll parameters. We consider Planck and 21 cm data independently, so the combined Fisher matrix is the sum of the contributions,

$$\mathbf{F}_{sr}^{tot} = \mathbf{F}_{sr}^{21cm} + \mathbf{F}_{sr}^{Planck}, \quad (23)$$

which we use to construct a χ^2 function,

$$\chi^2(\boldsymbol{\lambda}_{sr}) = \boldsymbol{\delta}_{\boldsymbol{\lambda}_{sr}}^T \mathbf{F}_{sr}^{tot} \boldsymbol{\delta}_{\boldsymbol{\lambda}_{sr}}, \quad (24)$$

where $\boldsymbol{\delta}$ denotes the deviations from the fiducial values of the slow-roll parameters.

6 Results

We forecast constraints on the slow-roll parameters at the fiducial points of Table 1 that are consistent with WMAP5 results. To supplement the uncertainties listed in the table, we provide the corresponding (approximate) uncertainties for the more familiar spectral parameters. The joint SKA+Planck (FFTT+Planck) analysis gives the 1σ uncertainties $\delta n_s = 0.0031$, $\delta\alpha = 0.0032$ ($\delta n_s = 6 \times 10^{-4}$, $\delta\alpha = 2.7 \times 10^{-4}$). These results roughly apply to all the classes of models in Section 4. These uncertainties are larger, but consistent with those in Ref. [21] since we marginalize over all other parameters, while in Ref. [21], r and α are held fixed in computing uncertainties for

Model	Fiducial	1σ (Planck alone)	1σ (SKA+Planck)	1σ (FFTT+Planck)
High ϵ				
1 parameter, ϵ	0.0071	6.9×10^{-4}	6.3×10^{-4}	6.9×10^{-5}
2 parameter, ϵ	0.0053	0.0014	0.0014	0.0012
η	-0.013	0.0034	0.0033	0.0026
3 parameter, ϵ	0.0063	0.0015	0.0015	0.0014
η	0.0069	0.0036	0.0033	0.0028
ξ	0.00083	0.0026	0.0016	1.6×10^{-4}
Low ϵ				
2 parameter, ϵ	10^{-8}	—	—	—
η	-0.027	0.0016	0.0014	1.5×10^{-4}
3 parameter, ϵ	10^{-8}	—	—	—
η	-0.0069	0.0024	0.0016	2.2×10^{-4}
ξ	0.002	0.0026	0.0016	1.4×10^{-4}

Table 1: Uncertainties on slow-roll parameters for models classified according to the size of ϵ . The fiducial values at the time of horizon-crossing are chosen to be consistent with the 2σ ranges favored by WMAP5 data [1].

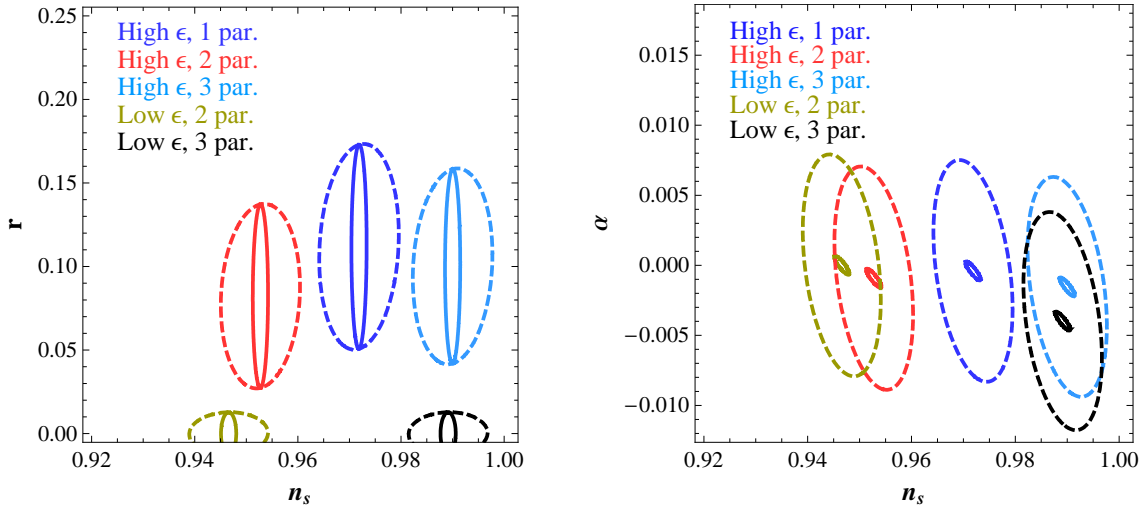


Figure 1: 2σ forecasts for the fiducial points in Table 1 from a Fisher matrix analysis of SKA+Planck (dashed) and FFTT+Planck (solid) in the (n_s, r) and (n_s, α) planes.

n_s , and r is fixed in computing uncertainties for α . For r large enough to be measured by Planck, $\delta r|_{r\sim 0.1} = 0.022$ and if r is tiny, a bound $\delta r|_{r\sim 0} = 0.005$ can be placed at 1σ . 21 cm data do not add any information on tensor modes. Figure 1 shows this information pictorially. The fiducial points are chosen so that the allowed regions have minimal overlap. A comparison of the constraints from the joint analyses with that from Planck data alone is shown in Fig. 2. The constraining power of 21 cm data comes from their sensitivity to n_s and particularly α . 21 cm and Planck data are complementary in their sensitivity to α and r .

It should be mentioned that higher order corrections to the brightness temperature power

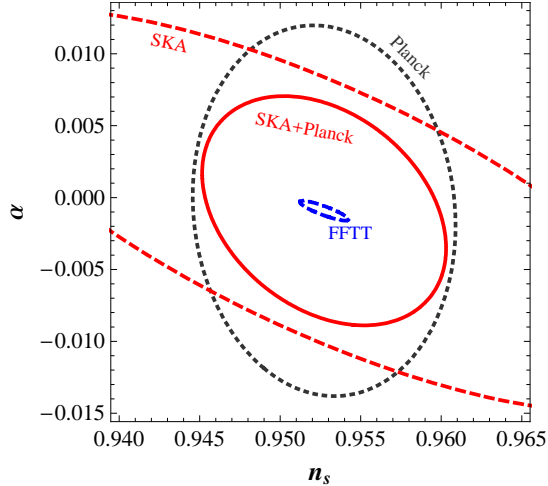


Figure 2: The impact of 21 cm experiments on parameter estimation. 2σ regions from an analysis of Planck alone, 21 cm alone, and 21 cm+Planck. The fiducial point for the high ϵ two-parameter model is used. FFTT and Planck are complementary: FFTT has good sensitivity to α but no sensitivity to r and Planck has good sensitivity to r but not α . We do not show the FFTT+Planck ellipse since it is indistinguishable from the ellipse for FFTT alone.

spectrum (Eqs. 15 – 20) may lead to errors as large as $\mathcal{O}(1)$ in the power spectrum at small scales $k \gtrsim 1 h \text{Mpc}^{-1}$ when the neutral fraction is $\langle x_H \rangle \sim 0.5$ [22]. However, since interferometer array measurements are more sensitive to small k modes than to large k modes because of thermal noise, cosmological constraints depend only weakly on k_{max} , the nonlinear cutoff scale above which we ignore 21 cm contributions to cosmology. Figure 6 of Ref. [21] shows that in their setup, the uncertainty in the tilt measured by the FFTT and the Planck data varies from roughly 0.0003 to 0.0006 to 0.0009 as k_{max} is reduced from 2Mpc^{-1} to 1Mpc^{-1} to 0.6Mpc^{-1} . Regardless of the exact value of k_{max} that can be determined by further careful modeling, it is qualitatively robust that cosmological constraints from FFTT and Planck data will reach unprecedented precision, *e.g.*, the measurement of n_s at the level of 10^{-4} .

To implement Monte Carlo reconstruction of the potential, we randomize slow-roll parameters inside the 2σ regions allowed by 21 cm+Planck data as the values when the scale k_0 left the horizon. We then evolve Eqs. (6) and (7) forward in time. Those cases are selected in which inflation ends with the number of e-folds N that pass a prior $N_{\text{min}} < N < N_{\text{max}}$. The prior on N is necessary because (i) a sufficiently large N is required to be consistent with the observed horizon size; (ii) a small N indicates relatively fast rolling which suggests that higher-order parameters may not be small enough to be truncated; (iii) a large N indicates that rolling is extremely slow so that a hybrid mechanism might be responsible for end the inflation. While our framework supposes that observable inflation is dominated by a single scalar field, it does not preclude the possibility of a hybrid transition caused by other fields ending inflation. We use two priors, $40 < N < 70$ and

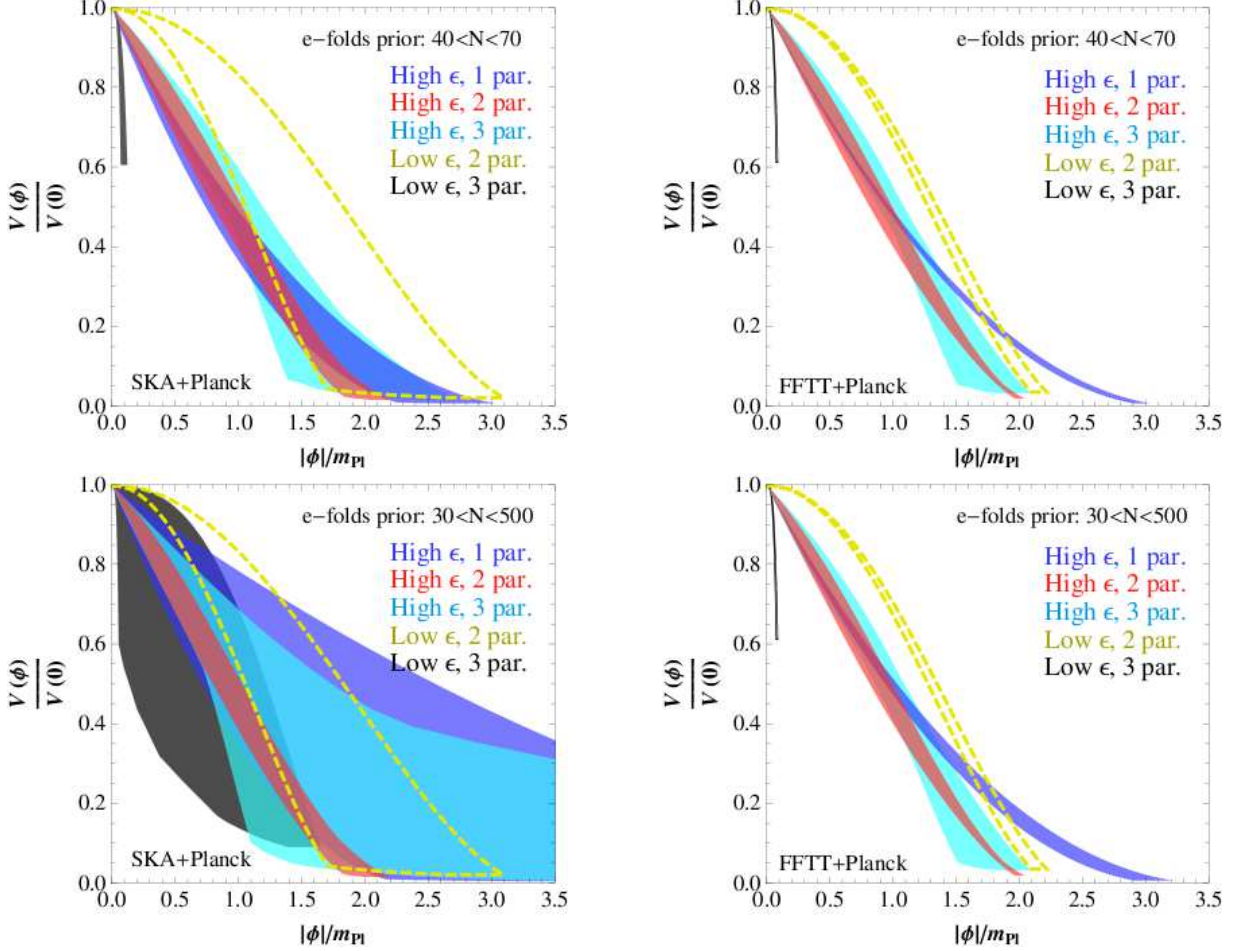


Figure 3: Bands of reconstructed potentials at 2σ from SKA+Planck (left) and FFTT+Planck (right) for two sets of priors on the number of e-folds, $40 < N < 70$ (upper) and $30 < N < 500$ (lower). Note that the low ϵ two-parameter model requires $N > 180$ and is eliminated by the $40 < N < 70$ prior. The unshaded bands in the upper panels are shown only for comparison. It is remarkable that the reconstruction using FFTT+Planck is barely affected by the e-fold prior. The enlarged SKA+Planck band for the low ϵ three-parameter model for $30 < N < 500$ is a consequence of $\xi \simeq 0$ being allowed at 2σ .

$30 < N < 500$. The first prior is typical for a plausible expansion history of our universe with Ref. [35] arguing for N between 50 and 60. This first prior does not account for a hybrid transition. Our second prior is rather conservative $30 < N < 500$, with the large values suggesting that some other mechanism brings an abrupt end to inflation.

In Fig. 3, the bands show the envelopes of possible potentials at the 2σ C. L. for each class of models with fiducial values as in Table 1. The envelopes capture the shapes of the potentials because the reconstructed potentials do not show any fine dependence on ϕ . While the reconstruction from SKA+Planck is clearly affected by the e-fold prior, it is striking that the reconstruction from FFTT+Planck is essentially unaffected. The low ϵ two-parameter model is inconsistent with the

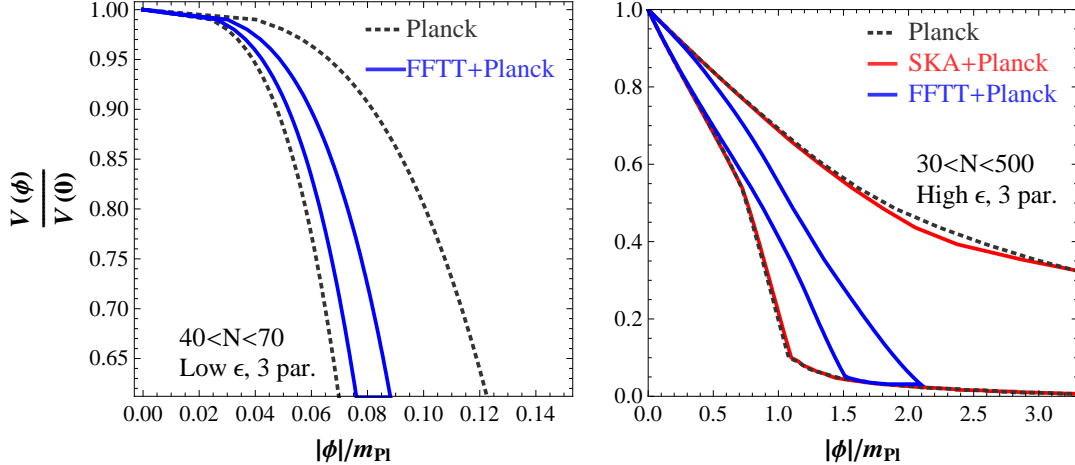


Figure 4: The impact of 21 cm experiments on potential reconstruction. 2σ bands from Planck alone and 21 cm+Planck. The left panel is a magnified view of the low ϵ three-parameter model; the SKA+Planck band is almost identical to that for Planck alone and is not shown.

$40 < N < 70$ prior since WMAP5 data yield $N > 180$ for these models. The SKA+Planck band for the low ϵ three-parameter model expands greatly for the $30 < N < 500$ prior because $\xi \simeq 0$ becomes allowed at 2σ . Note that detection of tensors by Planck is not sufficient to guarantee satisfactory potential reconstruction using Planck data alone. For example, FFTT data crucially improve the reconstruction of the high ϵ 1 parameter model. In Fig. 4, we compare results for models which require 3 slow-roll parameters for their description. FFTT data narrow down the 2σ bands considerably.

We conclude by emphasizing that a joint analysis of 21 cm measurements from FFTT with Planck data will significantly help pin down the slow-roll parameters and determine the shape of the inflationary potential. The improvement over the reconstruction using Planck data alone may stimulate major developments in our understanding of the particle physics responsible for inflation.

Acknowledgments

We thank Paul Shapiro and Max Tegmark for helpful suggestions. This research was supported by the DoE under Grant Nos. DE-FG02-95ER40896, DE-FG02-04ER41308 and DE-FC02-94ER40818, by the NSF under grant Nos. PHY-0544278 and AST-0708176, by NASA under grant Nos. NNX07AH09G and NNG04G177G, by Chandra grant No. SAO TM8-9009X, and by the Wisconsin Alumni Research Foundation.

References

- [1] G. Hinshaw *et al.* [WMAP Collaboration], arXiv:0803.0732 [astro-ph].
- [2] <http://www.rssd.esa.int/index.php?project=Planck>
- [3] A. D. Linde, Phys. Lett. B **129**, 177 (1983); P. J. Steinhardt and M. S. Turner, Phys. Rev. D **29** (1984) 2162.
- [4] A. Liddle, P. Parsons and J. Barrow, Phys. Rev. D **50**, 7222 (1994) [arXiv:astro-ph/9408015].
- [5] A. D. Linde, Phys. Lett. B **129**, 177 (1983).
- [6] A. D. Linde, Phys. Lett. B **108**, 389 (1982); A. Albrecht and P. J. Steinhardt, Phys. Rev. Lett. **48**, 1220 (1982); K. Freese, J. A. Frieman and A. V. Olinto, Phys. Rev. Lett. **65**, 3233 (1990).
- [7] A. D. Linde, Phys. Rev. D **49**, 748 (1994) [arXiv:astro-ph/9307002].
- [8] M. S. Turner, Phys. Rev. D **48**, 5539 (1993) [arXiv:astro-ph/9307035]; E. J. Copeland, E. W. Kolb, A. R. Liddle and J. E. Lidsey, Phys. Rev. D **48**, 2529 (1993) [arXiv:hep-ph/9303288]; A. R. Liddle and M. S. Turner, Phys. Rev. D **50**, 758 (1994) [Erratum-*ibid.* D **54**, 2980 (1996)] [arXiv:astro-ph/9402021].
- [9] J. Lesgourgues, A. A. Starobinsky and W. Valkenburg, JCAP **0801**, 010 (2008) [arXiv:0710.1630 [astro-ph]]; Q. G. Huang, Phys. Rev. D **76**, 043505 (2007) [arXiv:astro-ph/0610924]; H. Peiris and R. Easther, JCAP **0610**, 017 (2006) [arXiv:astro-ph/0609003]; J. Martin and C. Ringeval, JCAP **0608**, 009 (2006) [arXiv:astro-ph/0605367]; W. H. Kinney, E. W. Kolb, A. Melchiorri and A. Riotto, Phys. Rev. D **74**, 023502 (2006) [arXiv:astro-ph/0605338]; R. Easther and H. Peiris, JCAP **0609**, 010 (2006) [arXiv:astro-ph/0604214]; V. Barger, H. S. Lee and D. Marfatia, Phys. Lett. B **565**, 33 (2003) [arXiv:hep-ph/0302150].
- [10] R. Easther and W. H. Kinney, Phys. Rev. D **67**, 043511 (2003) [arXiv:astro-ph/0210345].
- [11] P. Adshead and R. Easther, arXiv:0802.3898 [astro-ph].
- [12] <http://www.haystack.mit.edu/ast/arrays/mwa/>
- [13] <http://21cma.bao.ac.cn/>, formerly known as the PaST (<http://web.phys.cmu.edu/~past/>).
- [14] <http://www.lofar.org/>
- [15] <http://gmrt.ncra.tifr.res.in/>

- [16] <http://astro.berkeley.edu/~dbacker/eor/>
- [17] <http://www.skatelescope.org/>
- [18] M. Tegmark and M. Zaldarriaga, arXiv:0805.4414 [astro-ph].
- [19] J. D. Bowman, M. F. Morales and J. N. Hewitt, *Astrophys. J.* **661**, 1 (2007) [arXiv:astro-ph/0512262]; M. McQuinn, O. Zahn, M. Zaldarriaga, L. Hernquist and S. R. Furlanetto, *Astrophys. J.* **653**, 815 (2006) [arXiv:astro-ph/0512263]; M. G. Santos and A. Cooray, *Phys. Rev.* **D74**,083517 (2006) [arXiv:astro-ph/0605677].
- [20] S. Wyithe, A. Loeb and P. Geil, arXiv:0709.2955 [astro-ph].
- [21] Y. Mao, M. Tegmark, M. McQuinn, M. Zaldarriaga and O. Zahn, *Phys. Rev. D* **78**, 023529 (2008) [arXiv:0802.1710 [astro-ph]].
- [22] A. Lidz, O. Zahn, M. McQuinn, M. Zaldarriaga and S. Dutta, *Astrophys. J.* **659**, 865 (2007) [arXiv:astro-ph/0610054].
- [23] B. A. Powell and W. H. Kinney, *JCAP* **0708**, 006 (2007) [arXiv:0706.1982 [astro-ph]].
- [24] J. E. Lidsey, A. R. Liddle, E. W. Kolb, E. J. Copeland, T. Barreiro and M. Abney, *Rev. Mod. Phys.* **69**, 373 (1997) [arXiv:astro-ph/9508078].
- [25] W. H. Kinney, *Phys. Rev. D* **66**, 083508 (2002) [arXiv:astro-ph/0206032].
- [26] A. R. Liddle, *Phys. Rev. D* **68**, 103504 (2003) [arXiv:astro-ph/0307286].
- [27] H. V. Peiris *et al.* [WMAP Collaboration], *Astrophys. J. Suppl.* **148**, 213 (2003) [arXiv:astro-ph/0302225].
- [28] Planck Collaboration, arXiv:astro-ph/0604069.
- [29] S. Furlanetto, S. P. Oh and F. Briggs, *Phys. Rept.* **433**, 181 (2006) [arXiv:astro-ph/0608032].
- [30] G. B. Field, *Astrophys. J.* **129**, 525 (1959).
- [31] S. Furlanetto, M. Zaldarriaga and L. Hernquist, *Astrophys. J.* **613**, 1 (2004) [arXiv:astro-ph/0403697]; M. G. Santos, A. Cooray and L. Knox, *Astrophys. J.* **625**, 575 (2005) [arXiv:astro-ph/0408515]; M. Zaldarriaga, S. R. Furlanetto and L. Hernquist, *Astrophys. J.* **608**, 622 (2004) [arXiv:astro-ph/0311514]; R. Barkana and A. Loeb, *Astrophys. J.* **626**, 1 (2005) [arXiv:astro-ph/0410129]; J. R. Pritchard and S. R. Furlanetto, *Mon. Not. Roy. Astron. Soc.* **376**, 1680 (2007) [arXiv:astro-ph/0607234].

- [32] A. Nusser, *Mon. Not. Roy. Astron. Soc.* **364**, 743 (2005) [arXiv:astro-ph/0410420]; R. Barkana, *Mon. Not. Roy. Astron. Soc.* **372**, 259 (2006) [arXiv:astro-ph/0508341].
- [33] M. Tegmark, A. Taylor and A. Heavens, *Astrophys. J.* **480**, 22 (1997) [arXiv:astro-ph/9603021].
- [34] A. Lewis, A. Challinor and A. Lasenby, *Astrophys. J.* **538**, 473 (2000) [arXiv:astro-ph/9911177]. Available at <http://camb.info/>
- [35] A. R. Liddle and S. M. Leach, *Phys. Rev. D* **68**, 103503 (2003) [arXiv:astro-ph/0305263].